arXiv:2210.00279v3 [math.NA] 16 Jan 2023

FAILURE-INFORMED ADAPTIVE SAMPLING FOR PINNS

ZHIWEI GAO, LIANG YAN, AND TAO ZHOU

Abstract. Physics-informed neural networks (PINNs) have emerged as an effective technique for solving PDEs in a wide range of domains. It is noticed, however, the performance of PINNs can vary dramatically with different sampling procedures. For instance, a fixed set of (prior chosen) training points may fail to capture the effective solution region (especially for problems with singularities). To overcome this issue, we present in this work an adaptive strategy, termed the failure-informed PINNs (FI-PINNs), which is inspired by the viewpoint of reliability analysis. The key idea is to define an effective failure probability based on the residual, and then, with the aim of placing more samples in the failure region, the FI-PINNs employs a failure-informed enrichment technique to adaptively add new collocation points to the training set, such that the numerical accuracy is dramatically improved. In short, similar as adaptive finite element methods, the proposed FI-PINNs adopts the failure probability as the posterior error indicator to generate new training points. We prove rigorous error bounds of FI-PINNs and illustrate its performance through several problems.

1. Introduction

Partial differential equations (PDEs) are important tools for modeling many real-world phenomena. Traditional numeric solvers such as finite difference method and finite element method have been widely used to solve PDEs for many decades. However, for high-dimensional problems, the computational cost will be prohibitively expensive when applying those methods due to the dramatic increase in the number of grids and thus the curse of dimensionality is inevitable. Driven by their well-documented performance in fields of machine learning, particularly deep learning is being increasing used in scientific computing. As a result, the area of scientific machine learning has emerged, see e.g., [4, 5, 17, 18, 26].

Physics-Informed neural networks (PINNs) [15, 17] is one of the popular machine learning methods for solving PDEs with deep neural networks. PINNs adopt automatic differentiation to solve PDEs by penalizing the PDE in the loss function at a random set of points in the domain of interest. PINNs have been successfully applied to simulate a variety of forward and inverse problems for PDEs, see [22, 12, 15, 8, 9] and references therein. Being a mesh less approach, a key issue in PINNs is how to choose the training points. Obviously, for PDEs with complex solution structures, a fixed set of (prior chosen) training points may fail to capture the effective solution region [14, 22, 23]. Another limitation is that when implementing PINNs to PDEs in an unbounded domain, due to the lack of prior knowledge

School of Mathematics, Southeast University, Nanjing 210096, China.

School of Mathematics, Southeast University, Nanjing 210096; Nanjing Center for Applied Mathematics, Nanjing 211135, China. Email: yanliang@seu.edu.cn. L. Yan is supported by NSF of China (No.11771081).

LSEC, Institute of Computational Mathematics, Academy of Mathematics and Systems Science, Chinese Academy of Sciences, Beijing 100190, China. Email: tzhou@lsec.cc.ac.cn. T. Zhou is partially supported by the National Key R&D Program of China(No. 2020YFA0712000), the NSF of China (under grant numbers 11822111, 11688101and 11731006), the Strategic Priority Research Program of Chinese Academy of Sciences (No. XDA25000404) and youth innovation promotion association (CAS).

about the PDE solutions, choosing an effective training set can be challenging. To address these issues, some adaptive sampling strategies have been proposed [3, 7, 15, 19, 20, 6], see also a recent review [24]. Among others, the most common strategy is the residual-based adaptive refinement method (RAR) in [15]. The RAR method provides an insight to adaptively select samples based on residual errors. However, the adaptive samples in RAR are chosen based on a large set of candidate points (either grid-based or sampled with a prior distribution), making it not effective for high dimensional problems. Another interesting idea is the so-called deep adaptive sampling (DAS) method [20], in which one first train a generative model based on the residual, and then the generative model can be used to generate new training points. While DAS is certainly a more general approach, however, the main issue for DAS is that the complexity for training a generative model can be comparable for solving the PDEs.

Motivated by the above discussions, we present in this work the failure-informed PINNs (FI-PINNs) that can effectively generate adaptive training points. Our approach is inspired by the viewpoint of reliability analysis. The key idea is to define an effective failure probability based on the residual, and then, with the aim of placing more samples in the failure region, the FI-PINNs employs a failure-informed enrichment technique to adaptively add new collocation points to the training set, in such a way that the numerical accuracy is dramatically improved. We summarize the main features of FI-PINNs as follows:

- In each iteration, based on the residual, we define the failure probability as an error indicator. This is similar as in the adaptive finite element methods, where one drive posterior error indicator for adjusting the meshes.
- In each iteration, we use the simple (truncated) Gaussian model to estimate the failure probability and to generate new training points, and this can be done in a very efficient way (compared to RAR and DAS).
- We prove rigorous error bound for FI-PINNs in terms of the error tolerance and failure probability tolerance.
- We test FI-PINNs for various PDE problems, which include PDEs with singular solutions, PDEs in unbounded domains, and time-dependent PDEs. It is shown that for all the test problems, FI-PINNs can effectively capture the solution structure.
- Our adaptive sampling strategy, especially the important sampling idea, may be extended to other formulations such as the deep Ritz method [5] and weak adversarial networks [26].

The rest of this paper is organized as follows. In the next section, we briefly introduces the basic knowledge of PINNs. In Section 3 we present FI-PINNs and propose the adaptive sampling strategy. In Section 4, we present the convergence analysis of FI-PINNs. Finally, we provide numerical experiments in Section 5, and this is followed by some concluding remarks in Section 6.

2. Preliminaries of PINNs

We briefly review physics-informed neural networks (PINNs). Let $\Omega \in \mathbb{R}^d$ be a spatial domain, and we denote by $\mathbf{x} \in \Omega$ the spatial variable. Consider the following partial

differential equations:

$$\begin{aligned} \mathcal{A}(\mathbf{x}; u(\mathbf{x})) &= 0, \quad \mathbf{x} \in \Omega, \\ \mathcal{B}(\mathbf{x}; u(\mathbf{x})) &= 0, \quad \mathbf{x} \in \partial\Omega, \end{aligned} \tag{1}$$

where $\mathcal{A}$ is a linear or non-linear differential operator, $\mathcal{B}$ is the boundary operator, and $u(\mathbf{x})$ is the unknown solution.

The basic idea of PINNs is to use a deep neural network (DNN) $u(\mathbf{x}; \theta)$ with parameters θ to approximate the unknown solution $u(\mathbf{x})$. The PDE solution is then obtained by choosing the best parameters for the following soft constrained optimization problem:

$$\min_{\theta \in \Theta} \mathcal{L}(\theta) = \min_{\theta \in \Theta} \mathcal{L}_c(\theta) + \lambda \mathcal{L}_b(\theta), \tag{2}$$

where Θ is the parameter space and λ is a penalty factor that balances the PDE loss $\mathcal{L}_c(\theta)$ and the boundary loss $\mathcal{L}_b(\theta)$. A common choice for $\mathcal{L}(\theta)$ is the L^2 loss, i.e.,

$$\mathcal{L}_c(\theta) = \|r(\mathbf{x}; \theta)\|^2_{2,\Omega}, \quad \mathcal{L}_b(\theta) = \|b(\mathbf{x}; \theta)\|^2_{2,\partial\Omega},$$

where $r(\mathbf{x}; \theta) = \mathcal{A}(\mathbf{x}; u(\mathbf{x}; \theta))$, and $b(\mathbf{x}; \theta) = \mathcal{B}(\mathbf{x}; u(\mathbf{x}; \theta))$ measure how well $u(\mathbf{x}, \theta)$ satisfies the PDE and the boundary operators, respectively. The above L^2-norm is defined as $\|u\|^2_{2,\Omega} = \int_\Omega u(\mathbf{x})^2 \omega(\mathbf{x}) d\mathbf{x}$, where $\omega(\mathbf{x})$ is a prior distribution and is usually set to be 1 when the problem domain is bounded.

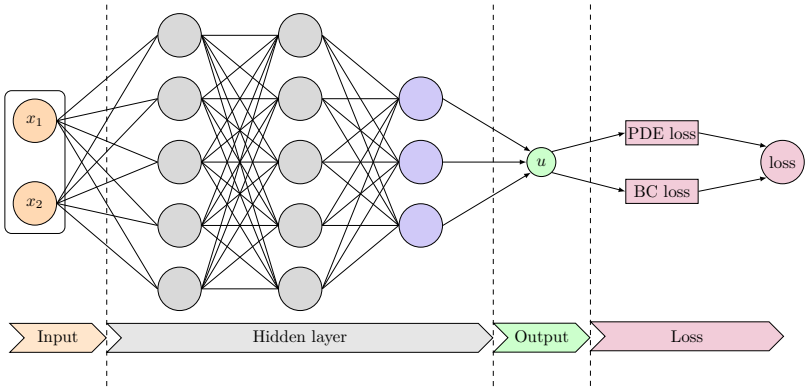


FIGURE 1. The framework of PINNs

We present in Fig.1 the general PINNs framework. In practice, the loss functional $\mathcal{L}(\theta)$ should be discretized by giving a prior distributed training dataset, which consists of the discrete points (collocation points) $\mathcal{D}_c = \{\mathbf{x}_i^c\}_{i=1}^{N_c}$ and the boundary points $\mathcal{D}_b = \{\mathbf{x}_i^b\}_{i=1}^{N_b}$. We can then consider the discrete loss function

$$\hat{\mathcal{L}}(\theta) = \hat{\mathcal{L}}_c(\theta) + \lambda \hat{\mathcal{L}}_b(\theta), \tag{3}$$

where

$$\hat{\mathcal{L}}_c(\theta) = \frac{1}{N_c} \sum_{i=1}^{N_c} |r(\mathbf{x}_i^c; \theta)|^2, \quad \hat{\mathcal{L}}_b(\theta) = \frac{1}{N_b} \sum_{i=1}^{N_b} \left| b(\mathbf{x}_i^b; \theta) \right|^2. \tag{4}$$

It should be noted that the penalty factor λ is often chosen as $\lambda = 1$ in most cases, but it can be carefully tuned to achieve better performance [22, 23]. The discrete loss function (3) can then be minimized using stochastic gradient-based algorithms [2, 13].

Although PINNs have been successfully applied to simulate a variety of forward and inverse problems for PDEs, they can sometimes have difficulty in converging to the true solution, as shown in several studies depicting the *failure modes* of PINNs [14, 22, 23]. These potential failure modes are caused by the mechanism of PINNs, which makes optimizing the loss function extremely difficult due to its complicated landscape. To address these challenges, specialized solutions have been proposed independently.

Modify the loss function. Modifying the structure of the loss function has become a popular tool for training PINNs. This includes (I) applying adaptive weights for each individual point [16], (II) embedding gradient information of the residual function in the total loss [25], and (III) combing the augmented Lagrangian relaxation to balance different loss components [10].

Construct new learning schemes. Recent ideas along this line include the extended PINNs (XPINNs) [11] and sequence to sequence learning[14].

Adaptive sampling strategies. Adaptive sampling strategies are essential for training PINNs [3, 7, 15, 19, 20, 24]. As discussed in the last section, [15] proposes to update the training dataset by selecting points from a uniformly distributed set with larger residual values. While [20] proposed to use the generative model, e.g., the KRnet, to generate the training points.

Our contribution belongs to the third category, i.e., we focus on developing an efficient adaptive sampling strategy for PINNs.

3. Failure-informed PINNs (FI-PINNs)

In this section, we introduce the concept of failure-informed PINNs. To this end, We shall first discuss how to establish an adaptive sampling framework from the view of reliability analysis, and then we shall present a self-adaptively importance sampling procedure in FI-PINNs.

To begin, we first define the so-called *limit-state function (LSF)* $g(\mathbf{x}) : \Omega \to \mathbb{R}$

$$g(\mathbf{x}) = \mathcal{Q}(\mathbf{x}) - \epsilon_r.$$

Here, ϵ_r is a predefined maximum allowed threshold, and $\mathcal{Q}(\mathbf{x}) : \Omega \to \mathbb{R}$ maps the domain to a quantity of interest (QoI) that characterizes the system's performance. In PINNs, we can simply choose $\mathcal{Q}(\mathbf{x}) = |r(\mathbf{x};\theta)|$ with $r(\mathbf{x};\theta)$ being the residual such that

$$g(\mathbf{x}) = |r(\mathbf{x};\theta)| - \epsilon_r. \tag{5}$$

The failure hypersurface defined by $g(\mathbf{x}) = 0$ divides the physics domain into two subsets: the safe set $\Omega_{\mathcal{S}} = \{\mathbf{x} : g(\mathbf{x}) < 0\}$ and the failure set $\Omega_{\mathcal{F}} = \{\mathbf{x} : g(\mathbf{x}) > 0\}$. To describe the reliability of the PINNs, we define the *failure probability* $P_{\mathcal{F}}$ under a prior distribution $\omega(\mathbf{x})$:

$$P_{\mathcal{F}} = \int_{\Omega} \omega(\mathbf{x}) \mathbb{I}_{\Omega_{\mathcal{F}}}(\mathbf{x}) d\mathbf{x}. \tag{6}$$

Here $\mathbb{I}_{\Omega_{\mathcal{F}}} : \Omega \to \{0, 1\}$ represents the indicator function, which takes values $\mathbb{I}_{\Omega_{\mathcal{F}}}(\mathbf{x}) = 1$ when $\mathbf{x} \in \Omega_{\mathcal{F}}$, and $\mathbb{I}_{\Omega_{\mathcal{F}}}(\mathbf{x}) = 0$ otherwise.

If the failure probability is smaller than a given tolerance ϵ_p, we say that PINNs are reliable; otherwise, the failure region indicates that the system is unreliable, and the performance of PINNs should be improved. Generally speaking, as the failure region gets smaller, the failure probability decreases, meaning that the system is becoming more reliable. Motivated by this fact, we may design adaptive strategies to add new training points from the failure region $\Omega_{\mathcal{F}}$ and retrain the PINNs if $P_{\mathcal{F}} > \epsilon_p$. The failure probability can thus be

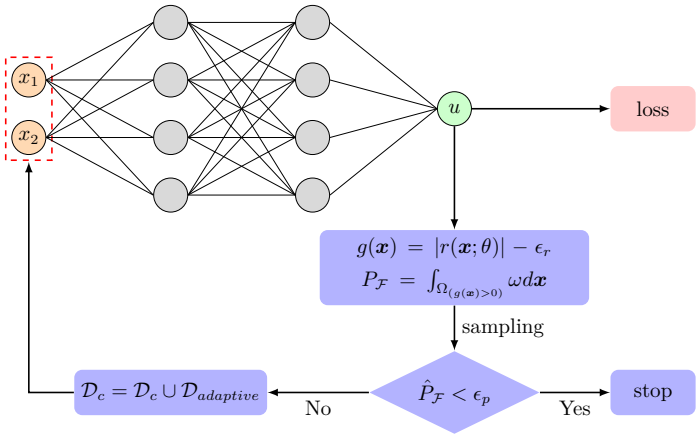


FIGURE 2. Workflow of FI-PINNs

Algorithm 1 Failure informed PINNs (FI-PINNs)

Require: A DNN solution $u(\mathbf{x};\theta)$, boundary points $\mathcal{D}_b$, collocation points $\mathcal{D}_c$. Maximum iterations M, residual tolerance ϵ_r and failure probability tolerance ϵ_p.

$s \leftarrow 1$.
while $s \leq M$ **do**
  Train $u(\mathbf{x};\theta)$ using the training dataset $\mathcal{D}_b, \mathcal{D}_c$.
  Set LSF g using Eq.(5).
  Estimate the failure probability $\hat{P}_{\mathcal{F}}$ using some sampling technique.
  if $\hat{P}_{\mathcal{F}} < \epsilon_p$ **then**
    Break
  end if
  Generate a new dataset $\mathcal{D}_{adaptive}$ from the failure region $\Omega_{\mathcal{F}}$.
  Set $\mathcal{D}_c = \mathcal{D}_c \cup \mathcal{D}_{adaptive}, s = s + 1$.
end while

used as a stopping indicator during the training of PINNs, similar as the posterior error indicator in adaptive finite element methods.

We present in Fig. 2 a general workflow of FI-PINNs, which can be used to combine with adaptive sampling strategies. The detailed algorithm of FI-PINNs is summarized in Algorithm 1. Notice that in Algorithm 1, the key issue is to estimate the failure probability $P_{\mathcal{F}}$ in Eq.(6), as the integral cannot be calculated analytically. Moreover, one needs also to design effective model to sampling the failure region in an efficient way. These two issues will be addressed in the forthcoming subsections.

3.1. **Monte Carlo and importance sampling.** To estimate the failure probability, a nature idea is to use the Monte Carlo (MC) methods. In this case, one may generate a set of randomly distributed locations $\mathcal{S} = \{\mathbf{x}_1, \mathbf{x}_2, \ldots, \mathbf{x}_{|\mathcal{S}|}\}$ from the prior $\omega(\mathbf{x})$ (e.g., the uniform distribution), then the Monte Carlo estimator is given by

$$\hat{P}_{\mathcal{F}}^{MC} = \frac{1}{|\mathcal{S}|} \sum_{\mathbf{x} \in \mathcal{S}} \mathbb{I}_{\Omega_{\mathcal{F}}}(\mathbf{x}).$$

Using this estimator, we can propose an adaptive sampling scheme. If $\hat{P}_{\mathcal{F}}^{MC} > \epsilon_p$, we add the new collocation points $\{\mathbf{x}_i\}$ which satisfy $\{\mathbf{x}_i : \mathbf{x}_i \in \mathcal{S},\, g(\mathbf{x}_i) > 0\}$ into the training set and retrain the network. Notice that in each iteration, the number of the new training points m may be different; it is determined by the number of points $\{\mathbf{x}_i\} \in \mathcal{S}$ that fall in the failure region $\Omega_{\mathcal{F}}$. The residual-based adaptive refinement (RAR) method [15] proposed to select a fixed number of m new points with the largest values of LSF g in $\mathcal{S}$.

Since the failure region may be relatively small compared to the entire problem domain, the above MC sampling strategy can be ineffective in generating effective samples. This is especially true when the PDEs exhibit local behaviors (e.g., in presence of sharp, or very localized features). Consequently, the sample size $|\mathcal{S}|$ is typically in the range of $\mathcal{O}(10^4 \sim 10^6)$, meaning that the procedure is extremely expensive.

Importance sampling (IS) can be considered to generate effective samples as it can reduce variance by selecting appropriate proposal distributions. In this case, we have

$$P_{\mathcal{F}} = \int_{\Omega} \mathbb{I}_{\Omega_{\mathcal{F}}}(\mathbf{x}) \frac{\omega(\mathbf{x})}{h(\mathbf{x})} h(\mathbf{x}) d\mathbf{x} = \mathbb{E}_h \left[\mathbb{I}_{\Omega_{\mathcal{F}}}(\mathbf{x}) R(\mathbf{x}) \right], \tag{7}$$

where $h(\mathbf{x})$ is the proposal distribution. Here $R(\mathbf{x})$ represents the weight function $\frac{\omega(\mathbf{x})}{h(\mathbf{x})}$ that transfers the proposal distribution $h(\mathbf{x})$ to the prior distribution $\omega(\mathbf{x})$. By choosing a set of randomly distributed samples $\mathcal{S} = \{\mathbf{x}_1, \mathbf{x}_2, \ldots, \mathbf{x}_{|\mathcal{S}|}\}$ from the proposal distribution h, we can approximate the failure probability $P_{\mathcal{F}}$ as

$$\hat{P}_{\mathcal{F}}^{IS} = \frac{1}{|\mathcal{S}|} \sum_{\mathbf{x} \in \mathcal{S}} \mathbb{I}_{\Omega_{\mathcal{F}}}(\mathbf{x}) R(\mathbf{x}). \tag{8}$$

If the support of h contains the intersection of the support of ω and the failure set, (8) gives an unbiased estimator for $P_{\mathcal{F}}$. Theoretically, there exists an optimal proposal distribution,

$$h_{opt}(\mathbf{x}) = \frac{\mathbb{I}_{\Omega_{\mathcal{F}}(\mathbf{x})} \omega(\mathbf{x})}{P_{\mathcal{F}}} = \frac{\mathbb{I}_{g(\mathbf{x})>0} \omega(\mathbf{x})}{\int_{\Omega} \mathbb{I}_{g(\mathbf{x})>0} \omega(\mathbf{x}) d\mathbf{x}}, \tag{9}$$

which leads to a zero-variance estimator. However, $h_{opt}(\mathbf{x})$ is not available in practice due to the normalizing constant. Note that, the optimal IS density $h_{opt}(\mathbf{x})$ can be interpreted as a "posterior-failure" density of the collocation points given the occurrence of the failure set $\Omega_{\mathcal{F}}$, where the indicator function $\mathbb{I}_{\Omega_{\mathcal{F}}(\mathbf{x})}$ is the likelihood function, $\omega(\mathbf{x})$ is the prior density, and $P_{\mathcal{F}}$ is the evidence.

Although it is impossible to evaluate and sample directly from h_{opt}, this still serves as a guide for selecting an IS proposal distribution. We will provide a self-adaptive importance sampling (SAIS) method for approximating the posterior-failure density h_{opt} in the following section.

3.2. **Self-adaptive importance sampling (SAIS).** As discussed above, the optimal density h_{opt} in (9) is in general not available. Consequently, our strategy is to develop an adaptive procedure that begins with an initial proposal and iteratively updates the intermediate proposal using samples. For efficiency reason, we simply choose the intermediate proposal distributions h_k as truncated Gaussian restricted to Ω, denoted as $\mathcal{N}_T(\mu_k, \Sigma_k)$.

To establish the adaptive scheme, we first set the initial proposal distribution as $h_1(\mathbf{x}) = \omega(\mathbf{x})$. Then, at the k step, we generate N_1 samples $\{\mathbf{x}_i^k\}_{i=1}^{N_1}$ from $h_k(\mathbf{x})$ and sort these samples according to their LSF values in a descending order to obtain the candidate points set $\mathcal{D}_k := \{\widetilde{\mathbf{x}}_i^k\}_{i=1}^{N_1}$. Let $N_p = \lfloor p_0 N_1 \rfloor$ denotes the minimum number of samples used to approximate the optimal distribution h_{opt}, here $0 < p_0 < 1$ is a fixed parameter. Let N_η

represents the number of points where $\mathcal{D}_k$ falls in the failure region. We use this number as an indicator: if $N_\eta < N_p$, this means that the intermediate proposal distribution h_k needs to be refined. Otherwise, if N_η is bigger than N_p, it means that the number of points is acceptable and we just use those points to approximate the optimal distribution $\hat{h}_{opt}$.

To update h_k into h_{k+1}, we consider the truncated Gaussian model, and use the first N_p samples to estimate the mean vector and the covariance matrix of h_{k+1} as follow:

$$\begin{aligned} \mu_{k+1} &= \frac{1}{N_p}\sum_{i=1}^{N_p}\widetilde{\mathbf{x}}_i^k, \\ \Sigma_{k+1} &= \frac{1}{N_p-1}\sum_{i=1}^{N_p}(\widetilde{\mathbf{x}}_i^k-\mu_{k+1})\otimes(\widetilde{\mathbf{x}}_i^k-\mu_{k+1}). \end{aligned} \tag{10}$$

Notice that this procedure can be done in a very efficient way.

Notice also that once the iterative scheme stopped, the mean vector μ_{opt} and the covariance matrix Σ_{opt} are approximated using the first N_p samples from the last iteration:

$$\begin{aligned} \mu_{opt} &= \frac{\sum_{i=1}^{N_p}\widetilde{\mathbf{x}}_i\omega(\widetilde{\mathbf{x}}_i)}{\sum_{i=1}^{N_p}\omega(\widetilde{\mathbf{x}}_i)} \\ \Sigma_{opt} &= \frac{1}{N_p-1}\sum_{i=1}^{N_p}(\widetilde{\mathbf{x}}_i-\mu_{opt})\otimes(\widetilde{\mathbf{x}}_i-\mu_{opt}). \end{aligned} \tag{11}$$

Thus, the approximated optimal distribution $\hat{h}_{opt}(\mathbf{x})$ is a truncated Gaussian with mean vector μ_{opt} and covariance matrix Σ_{opt}. By generating N_2 samples from $\hat{h}_{opt}$, the failure probability can be approximated as

$$\hat{P}_{\mathcal{F}}^{SAIS} = \frac{1}{N_2}\sum_{i=1}^{N_2}\frac{\omega(\mathbf{x}_i)}{\hat{h}_{opt}(\mathbf{x}_i)}\mathbb{I}_{\Omega_{\mathcal{F}}}(\mathbf{x}_i). \tag{12}$$

We present in Algorithm 2 the summary of the self-adaptive importance sampling (SAIS) procedure. In our experiments, we observe that by selecting $p_0 = 0.1$, SAIS can self terminate rapidly with high numerical accuracy.

Remark 1: The above strategy can be easily applied to time-dependent problems and problems in unbounded domains. For instance, when Ω is unbounded, the intermediate proposal distribution can be simply chosen as Gaussian, which has the same form with the prior distribution ω (see our numerical experiments in Section 5). Moreover, in this work, we simply consider a truncated Gaussian distribution to approximate the "posterior failure" density h_{opt}. One can easily generalize the truncated Gaussian model into more complex models such as the Gaussian mixture model; see Appendix A.1. The optimal choice of the "posterior failure" density h_{opt} will be part of our future works.

Remark 2: It is important to note that our FI-PINNs framework supports a wide range of performance functions. Despite the fact that we only pay attention to the residual function, it is easy to generalize to other concepts, such as its gradient function or causality-based weighted residual[21]; see also Appendix A.2.

4. Convergence analysis

This section is devoted to the convergence analysis of FI-PINNs. We shall need the following assumptions.

Algorithm 2 Self-adaptive importance sampling (SAIS)

Require: Number of samples N_1 and N_2, the parameter p_0, the LSF g, the prior distribution ω and the maximum updated number M.

$k \leftarrow 1$, set $h_1 = \omega$
while $k \leq M$ **do**
  Generate N_1 samples $\{\mathbf{x}_i\}_{i=1}^{N_1}$ from h_k.
  Sort the samples according to the corresponding LSF in a descending order to obtain $\widetilde{\mathbf{x}}_1, \ldots, \widetilde{\mathbf{x}}_{N_1}$.
  Let $N_\eta = \max_{1\leq i\leq N_1}\{i|g(\widetilde{\mathbf{x}}_i) > 0\}$ and $N_p = \lfloor p_0 N_1 \rfloor$.
  if $N_\eta < N_p$ **then**
    Compute μ_{k+1} and Σ_{k+1} using Eq.(10).
    Set $h_{k+1} = \mathcal{N}_T(\mu_{k+1}, \Sigma_{k+1})$.
    $k \leftarrow k + 1$.
  else
    Break
  end if
end while
Compute μ_{opt} and Σ_{opt} using (11).
Generate N_2 samples $\mathcal{S} = \{\mathbf{x}_1, \cdots, \mathbf{x}_{N_2}\}$ from $\mathcal{N}_T(\mu_{opt}, \Sigma_{opt})$.
Calculate $\hat{P}_{\mathcal{F}}^{SAIS}$ using Eq.(12).
return $\hat{P}_{\mathcal{F}}^{SAIS}, \mathcal{D}_{adaptive} = \{\mathbf{x}_i|g_k(\mathbf{x}_i) > 0,\, \mathbf{x}_i \in \mathcal{S}\}$.

Assumption 4.1. *Let $\mathcal{A}$ be a linear operator that maps $\mathcal{X} \to \mathcal{X}$ in problem* (1)*, where $\mathcal{X} \subset \Omega$ is a Hilbert space. We assume that the operator $\mathcal{A}$ and the boundary operator $\mathcal{B}$ satisfy*

$$C_1\|v\|_{2,\Omega} \leq \|\mathcal{A}v\|_{2,\Omega} + \|\mathcal{B}v\|_{2,\partial\Omega} \leq C_2\|v\|_{2,\Omega}, \quad \forall v \in \mathcal{X} \tag{13}$$

where the positive constants C_1 and C_2 are independent of v.

Assumption 4.2. *Assume the neural network $u(\mathbf{x};\theta)$ can be sufficiently trained to ensure that the residual function is bounded, which is $M := \max_{\mathbf{x}\in\Omega}|r(\mathbf{x};\theta^*)| < \infty$, and that for any ϵ_b,*

$$\big\|\mathcal{B}(u(\mathbf{x}) - u(\mathbf{x};\theta^*))\big\|_{2,\partial\Omega} \leq \epsilon_b. \tag{14}$$

Assumption 4.3. *Suppose the residual function $r(\mathbf{x};\theta^*)$ induced by the network $u(\mathbf{x};\theta^*)$ is bounded, that is,*

$$M := \max_{\mathbf{x}\in\Omega}|r(\mathbf{x};\theta^*)| < \infty \tag{15}$$

Assumption 4.2 simply supposes that we have successfully approximated the boundary data. We are now ready to present the following theorem.

Theorem 4.4. *Assume the problem domain Ω is bounded, and let $u(\mathbf{x};\theta^*)$ be an FI-PINNs solution of* (1)*. Suppose Assumptions* (4.1)*,* (4.2) *and* (4.3) *are satisfied. Then the following error estimate holds*

$$\big\|u(\mathbf{x}) - u(\mathbf{x};\theta^*)\big\|_{2,\Omega} \leq \sqrt{2}C_1^{-1}\big(S_\Omega(M^2\epsilon_p + \epsilon_r^2) + \epsilon_b^2\big)^{\frac{1}{2}}, \tag{16}$$

where

$$M = \max_{\mathbf{x}\in\Omega}|r(\mathbf{x};\theta^*)|,$$

S_Ω is the area of Ω and ϵ_r, ϵ_p are the pre-given tolerances.

Proof. Let $v = u(\mathbf{x}) - u(\mathbf{x};\theta^*)$. Using Assumption 4.1, it can be shown that

$$\begin{aligned}
&\|u(\mathbf{x}) - u(\mathbf{x};\theta^*)\|_{2,\Omega} \\
&\leq C_1^{-1}\left(\|\mathcal{A}(u(\mathbf{x}) - u(\mathbf{x};\theta^*))\|_{2,\Omega} + \|\mathcal{B}(u(\mathbf{x}) - u(\mathbf{x};\theta^*))\|_{2,\partial\Omega}\right) \\
&= C_1^{-1}\left(\|r(\mathbf{x};\theta^*)\|_{2,\Omega} + \|\mathcal{B}(u(\mathbf{x}) - u(\mathbf{x};\theta^*))\|_{2,\partial\Omega}\right) \\
&\leq \sqrt{2}C_1^{-1}\left(\|r(\mathbf{x};\theta^*)\|_{2,\Omega}^2 + \|\mathcal{B}(u(\mathbf{x}) - u(\mathbf{x};\theta^*))\|_{2,\partial\Omega}^2\right)^{\frac{1}{2}}.
\end{aligned}$$

From Assumption 4.2, we have

$$\|u(\mathbf{x}) - u(\mathbf{x};\theta^*)\|_{2,\Omega} \leq \sqrt{2}C_1^{-1}\left(\|r(\mathbf{x};\theta^*)\|_{2,\Omega}^2 + \epsilon_b^2\right)^{\frac{1}{2}}. \tag{17}$$

For the bounded domain Ω, we have

$$\begin{aligned}
\|r(\mathbf{x};\theta^*)\|_{2,\Omega}^2 &= \int_\Omega r(\mathbf{x};\theta^*)^2 d\mathbf{x} \\
&= \int_{\Omega_\mathcal{F}} r(\mathbf{x};\theta^*)^2 d\mathbf{x} + \int_{\Omega_\mathcal{S}} r(\mathbf{x};\theta^*)^2 d\mathbf{x}.
\end{aligned}$$

Using the definition of the failure probability $P_\mathcal{F}$ on bounded domain, it can be shown that

$$P_\mathcal{F} = \int_\Omega \mathbb{I}_{\Omega_\mathcal{F}}(\mathbf{x}) d\mathbf{x} = \int_{\Omega_\mathcal{F}} d\mathbf{x} = \frac{S_{\Omega_\mathcal{F}}}{S_\Omega}, \tag{18}$$

where $S_\Omega, S_{\Omega_\mathcal{F}}$ denote the areas of $\Omega, \Omega_\mathcal{F}$ respectively. If $P_\mathcal{F} < \epsilon_p$, we have

$$S_{\Omega_\mathcal{F}} < S_\Omega \epsilon_p. \tag{19}$$

Thus,

$$\int_{\Omega_\mathcal{F}} r(\mathbf{x};\theta^*)^2 d\mathbf{x} \leq \max_{\mathbf{x}\in\Omega_\mathcal{F}} |r(\mathbf{x};\theta^*)|^2 S_{\Omega_\mathcal{F}} \leq M^2 S_\Omega \epsilon_p, \tag{20}$$

where $M = \max_{\mathbf{x}\in\Omega} |r(\mathbf{x};\theta^*)|$.

Note that in the safe region $\Omega_\mathcal{S}$, the PDE residual $|r(\mathbf{x};\theta)|$ satisfy $|r(\mathbf{x};\theta^*)| < \epsilon_r$, which implies

$$\int_{\Omega_\mathcal{S}} r(\mathbf{x};\theta^*)^2 d\mathbf{x} \leq \epsilon_r^2 S_{\Omega_\mathcal{S}} \leq S_\Omega \epsilon_r^2. \tag{21}$$

Combing Eq.(20) and Eq.(21), we can obtain

$$\|r(\mathbf{x};\theta^*)\|_{2,\Omega}^2 \leq S_\Omega(M^2\epsilon_p + \epsilon_r^2). \tag{22}$$

The desired result follows by substituting Eq.(22) into Eq.(17). □

5. Numerical experiments

In this section, we present several numerical experiments to verify the effectiveness of FI-FINNs.

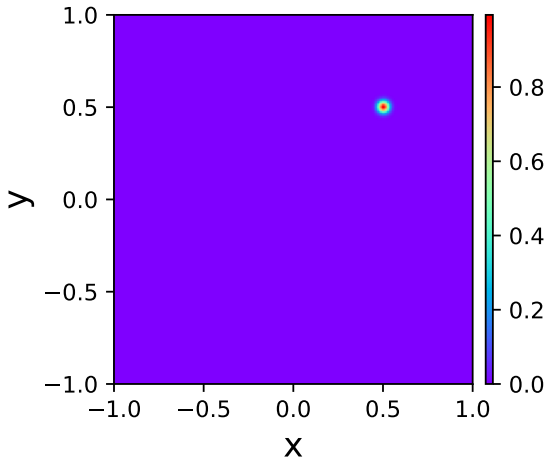


FIGURE 3. Exact solution for the two-dimensional peak test problem.

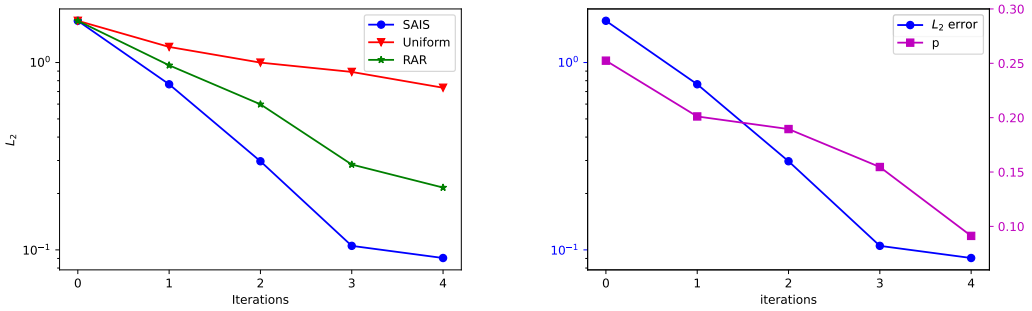


FIGURE 4. Relative L_2 error (left) and the estimated failure probability (right) over updates.

5.1. **Experiment Setup.** To better present the numerical results, we shall perform the following three types of approaches:

- The conventional PINNs [17], or baseline PINNs approach. This method update the training dataset by using the uniform sampling strategy.
- The residual-based adaptive refinement method (RAR) [15]. This method update the training set by selecting collocation points with the first (m) largest residual values, in a large set of candidate points.
- The FI-FINNs with SAIS presented in Section (3.1).

In all our numerical results, we will refer to "*Uniform*" as the traditional PINNs, "*RAR*" as the residual-based adaptive refinement approach, and "*SAIS*" as our FI-PINNs approach. To make a fair comparison, we shall first train the network completely using a small uniformly distributed dataset, and then we will train the three distinct models that are descended from the original model using datasets with the same size but produced using three different strategies.

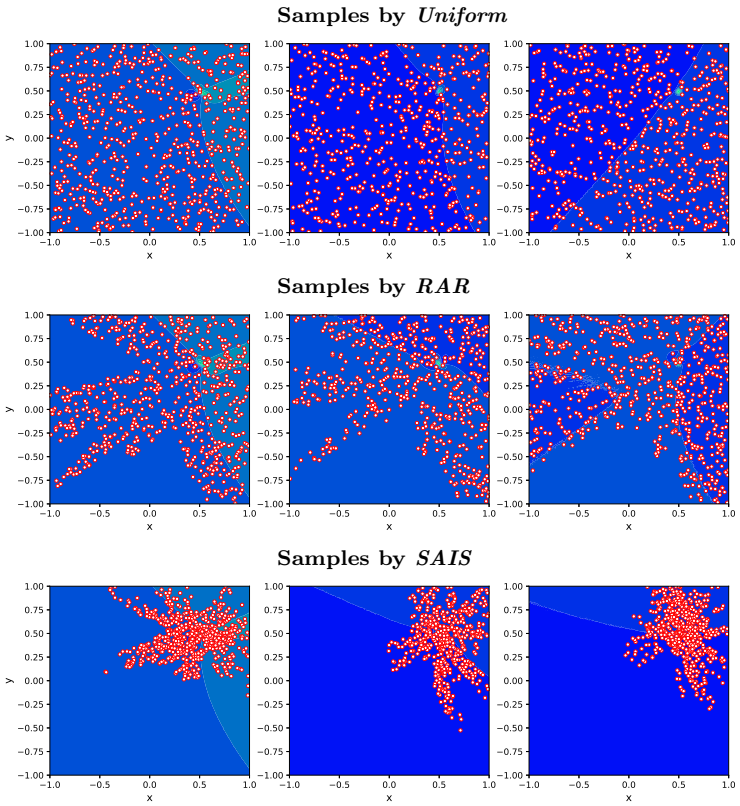


FIGURE 5. The distribution of collocation points obtained by three sampling methods for the first three updates.

Unless otherwise specified, we shall use the following parameters: $N_1 = 300, p_0 = 0.1, N_2 = 1000$ in *SAIS*. The network used to implement the experiments is a fully connected neural network with 7 hidden layers with 20 neurons in each layer, and the activation function is chosen as the `tanh` function. In the beginning, we always use 2000 collocation points and 200 boundary points to train the network. The `Adam` optimizer is adopted to optimize the loss function, with a learning rate 0.0001 and 10000 iterations. The maximum adaptive iteration is set to $M = 10$. In order to test the validity of the method, we use the following relative L_2 error:

$$err_{L_2} = \frac{\sqrt{\sum_{i=1}^{N} |\hat{u}(\mathbf{x}_i) - u(\mathbf{x}_i)|^2}}{\sqrt{\sum_{i=1}^{N} |u(\mathbf{x}_i)|^2}}, \tag{23}$$

where N represents the total number of test points chosen randomly in the domain, and $\hat{u}(\mathbf{x}_i)$ and $u(\mathbf{x}_i)$ represent the predicted and the exact solution values, respectively.

5.2. **Two-dimensional Poisson equation.** We first consider the following two-dimensional Poisson equation [20]:

$$\begin{aligned} -\Delta u(x,y) &= f(x,y) \quad \text{in } \Omega \\ u(x,y) &= g(x,y) \quad \text{on } \partial\Omega, \end{aligned} \tag{24}$$

where Ω is $[-1,1]^2$ and we specify the true solution as

$$u(x,y) = \exp\left(-1000\left[(x-0.5)^2 + (y-0.5)^2\right]\right), \tag{25}$$

which has a peak at $(0.5, 0.5)$ and decreases rapidly away from $(0.5, 0.5)$ (see Fig.3).

We first compare the numerical results obtained by three different sampling strategies. To construct our FI-PINNs framework, we set $\epsilon_p = 0.1$ and $\epsilon_r = 0.1$ in this example. The relative L_2 errors are shown in the left plot of Fig. 4. The error achieved by *SAIS* method decreases much faster than the *Uniform* and *RAR* strategies, and it is clearly seen that the mean L_2 error obtained by *SAIS* is much smaller, which is 9.04×10^{-2}, compared to 7.36×10^{-1} and 2.15×10^{-1} obtained by *Uniform* and *RAR* sampling strategies respectively. In the right plot of Fig. 4, we show that the estimated failure probability has the same trend with the relative L_2 error. After four iterations, the training can be stopped when the estimated failure probability is smaller than the tolerance, meaning that our stop criteria is effectiveness.

Fig.5 displays the distributions of the updated collocation points from the first three iterations using various sampling strategies. It is clear seen that the samples generated by *SAIS* are much more concentrated around the peak $(0.5, 0.5)$. The associated predicted values, absolute error and the predicted solution curve at $x = 0.5$ obtained by the three sampling strategies are shown in Fig.6. It is evident that the absolute error obtained by *SAIS* is much smaller, and there is hardy noticeable difference between the exact values and the predicted values at $x = 0.5$, indicating that the *SAIS* sampling strategy outperforms the other two sampling strategies.

We now examine the convergence properties of FI-PINNs. To show the convergence properties of FI-PINNs, we fix one tolerance parameter and train the network to obtain the prediction error when the other tolerance changes. The results are presented in Fig.7. It is clearly seen that the convergence rate with respect to ϵ_p and ϵ_r are $1/2$ and 1, respectively. This agrees well with Theorem 4.4.

5.3. **Burgers' equation.** We consider the following Burgers' equation:

$$\begin{aligned} &u_t + uu_x - \frac{0.01}{\pi} u_{xx} = 0, \\ &u(x, 0) = -\sin(\pi x), \\ &u(t, -1) = u(t, 1) = 0, \end{aligned} \tag{26}$$

where $(x, t) \in [-1, 1] \times [0, 1]$. Notice that there exists a stiff mutation at $x = 0$ in the solution, which is used here to test the viability of the FI-PINNs and the *SAIS* method for time-dependent nonlinear problems.

In this example, the residual tolerance ϵ_r and failure probability tolerance ϵ_p are both set to be 0.01. To implement the experiment, we first train the network using the `LBFGS` optimizer with a maximum of 50000 iterations. If the network needs to be updated (with new training points), we first retrain it using the `Adam` optimizer for a total of 10000 iterations, and then we utilize the `LBFGS` optimizer to fine tune the network with maximum 50000 iterations.

Figure 8 shows the prediction errors for three strategies, as well as the estimated failure probability with respect to iteration number. Again, it is clearly seen that the estimated failure probability and the prediction errors using *SAIS* have a similar pattern. The estimated failure probability is below the tolerance ϵ_p after four updates. Additionally, the prediction errors of *SAIS* are significantly lower (5.59×10^{-3}).

New training points generated in the first two iterations are presented in Fig. 9. We observe that the samples produced by the *SAIS* strategy are concentrated more in the regions where the residual error is high. In Fig.10, we show the final absolute prediction error as well as the predicted solution curve at the time $t = 1$. It is obvious that the

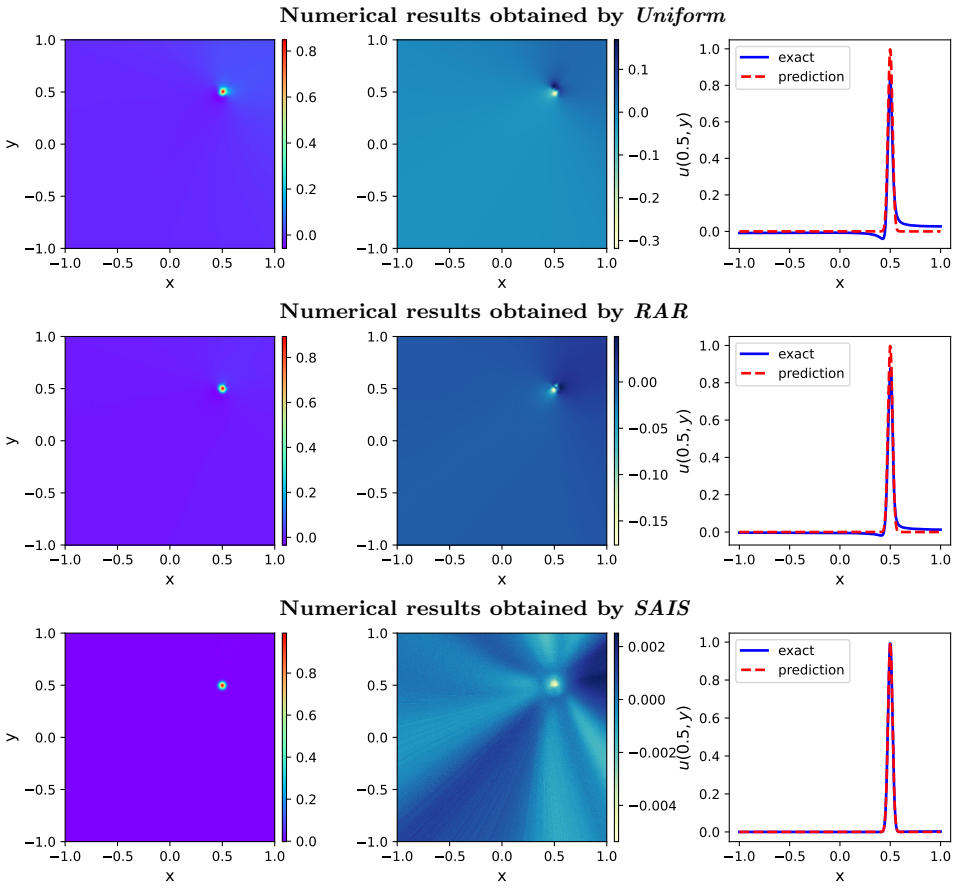


FIGURE 6. The predicted solution(Left), absolute error (Middle) and the predicted curves at $x = 0.5$(Right) obtained by the three different sampling strategies.

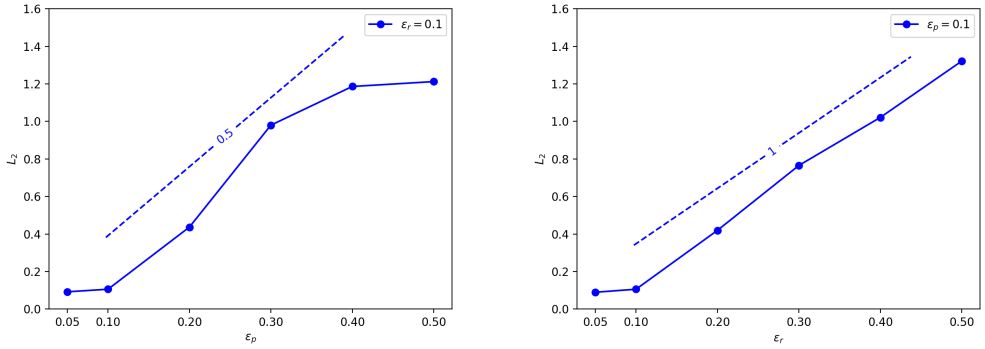


FIGURE 7. Error profiles when solving a 2D Poisson equation with one peak. Left: the prediction errors with respect to the ϵ_p with $\epsilon_r = 0.1$. Right: the prediction errors with respect to the ϵ_r with $\epsilon_p = 0.1$.

predicted values produced by the *SAIS* match well with the exact solution. Although we

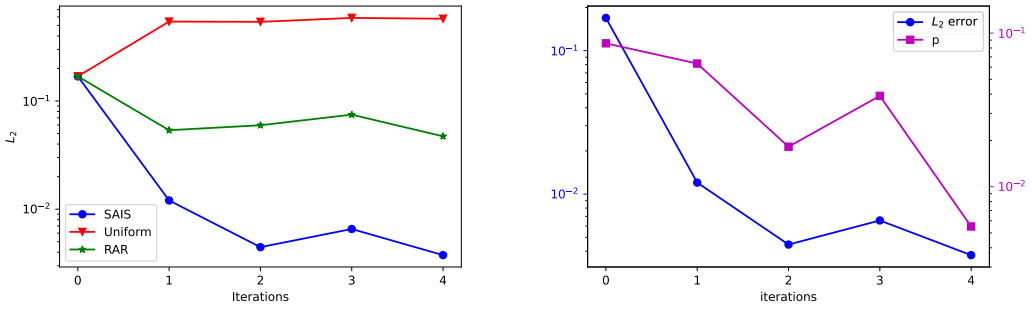


FIGURE 8. Relative L_2 error (left) and the estimated failure probability (right) over updates.

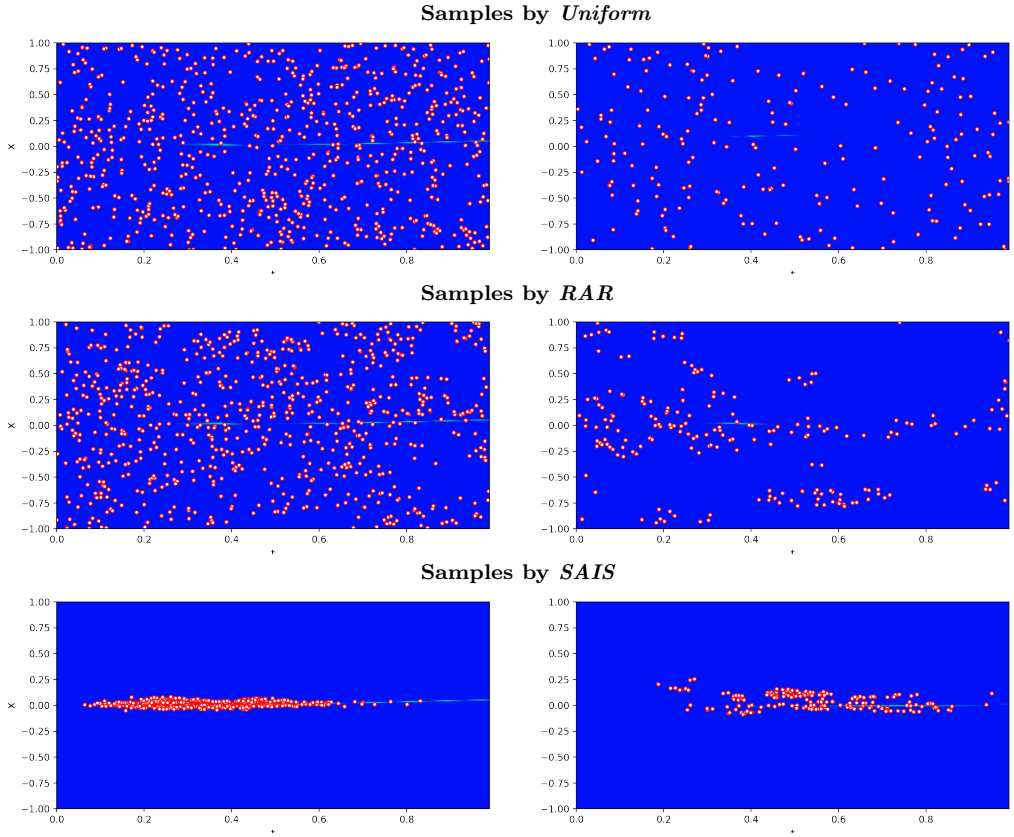


FIGURE 9. The distribution of collocation points obtained by three sampling methods for the first two updates.

have only established the theoretical results for the linear model. We indeed observe in Fig. 11 the convergence rates also hold for this nonlinear example.

5.4. **The high-dimensional Poisson equation.** Consider the the following d-dimensional elliptic equation

$$-\Delta u(\mathbf{x}) = f(\mathbf{x}), \quad \mathbf{x} \in [-1,1]^d,$$

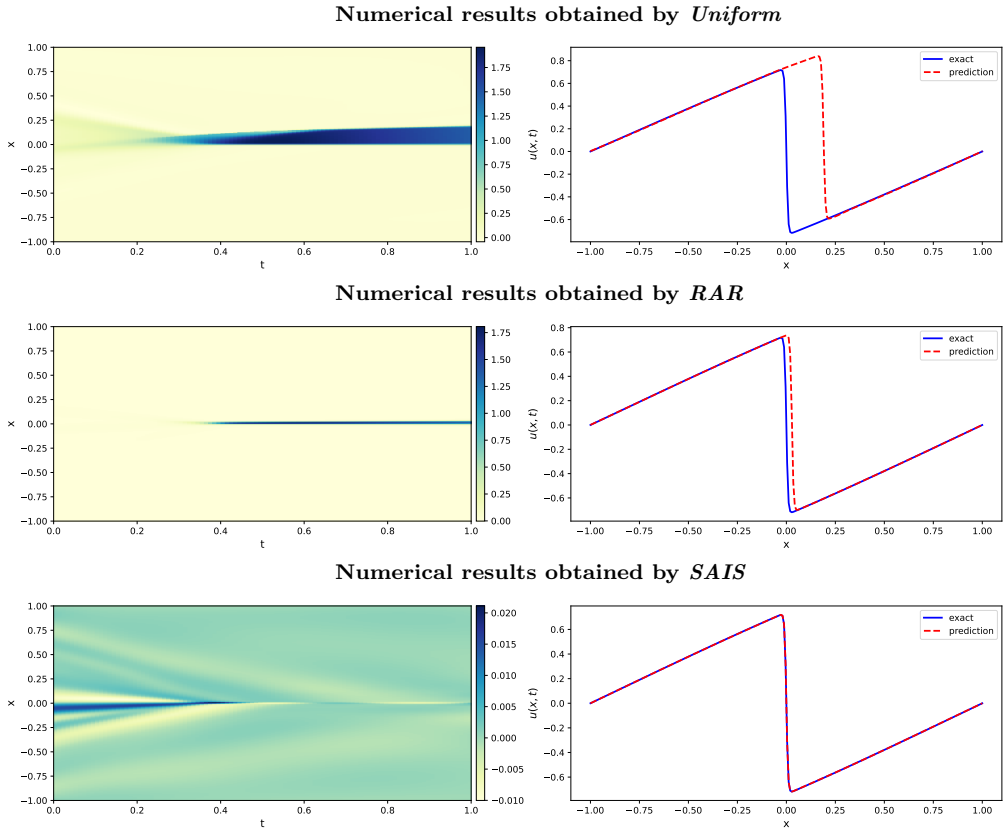


FIGURE 10. The predicted error (Left) and the predicted curves at $t = 1$(Right) obtained by the three different sampling strategies.

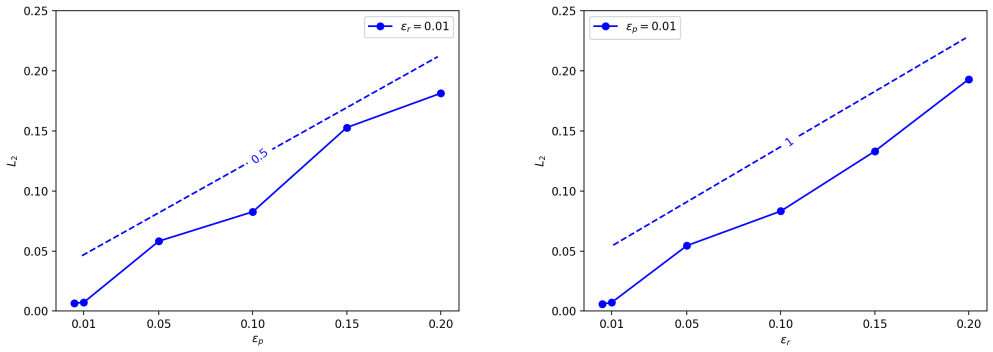


FIGURE 11. Errors profiles when solving Burgers' equation. Left: the prediction errors with respect to the ϵ_p with $\epsilon_r = 0.01$. Right: the prediction errors with respect to the ϵ_r with $\epsilon_p = 0.01$.

with an exact solution

$$u(\mathbf{x}) = e^{-10\|\mathbf{x}\|_2^2}.$$

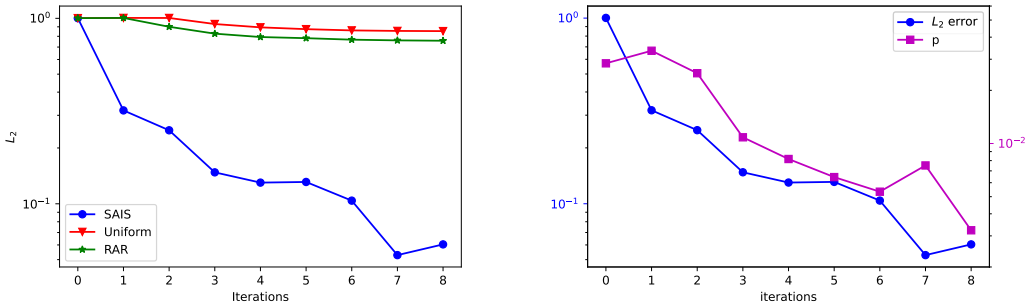


FIGURE 12. Relative L_2 error (left) and the estimated failure probability (Right); $d = 9$.

We set $d = 9$, and use 20000 collocation points and 900 boundary points to train the initial network. The hyperparameter for *SAIS* is set at $N_2 = 5000$. Additionally, we define the residual and failure probability tolerances as $\epsilon_r = 0.01, \epsilon_p = 0.005$ respectively.

The left plot of Fig. 12 displays the relative errors achieved using three different sampling strategies. It is shown that the error decreases smoothly when employing *SAIS*, whereas the *Uniform* and *RAR* seems not converge for this example. This demonstrates that *SAIS* can outperform other techniques in terms of efficiency. The right plot of Fig.12 further shows that the estimated failure probability has a similar trend with the mean L_2 error, confirming the efficiency of the stop criteria of FI-PINNs.

The new generated samples for the $2nd, 4th, 6th$ iterations in the space of x_8, x_9 are shown in Fig. 13. Again, it is clearly seen that the samples generated by *SAIS* are more concentrated around $(0, 0)$, which significantly increases the effective sample size to train the network and results in a smaller L_2 error; see also Fig.12.

5.5. **Two-dimensional unbounded problem.** Consider the following two-dimensional Possion problem

$$\begin{aligned} -\Delta u(x,y) &= f(x,y), \quad (x,y) \in \mathbb{R}^2 \setminus \Omega \\ u(x,y) &= s(x,y), \quad (x,y) \in \partial\Omega, \end{aligned} \tag{27}$$

where the true solution is

$$u(x,y) = e^{-(x-4)^2-(y-4)^2}. \tag{28}$$

The boundary of Ω is defined as

$$\partial\Omega = \left(\cos(t) - \frac{\cos(5t)\cos(t)}{4}, \sin(t) - \frac{\cos(5t)\sin(t)}{4}\right), \quad t \in [0, 2\pi].$$

In this unbounded example, we set the initial proposal distributions h_1 to be a two-dimensional Gaussian distribution with mean vector $\mu_1 = [0, 0]$, covariance matrix $\Sigma_1 = 3I_2$. Additionally, we set ϵ_r and ϵ_p in FI-PINNs to be 0.01 and 0.0001, respectively. We set the hyperparameter of the *SAIS* algorithm to $N_2 = 1000$.

The challenge of selecting a training data for unbounded domain arises from the fact that the true solution is unknown. To verify the effectiveness of our method, we starting with 5000 collocation points randomly chosen in $[-2, 2]^2 \setminus \Omega$ which is far away from the peak. The estimated failure probability becomes smaller than the tolerance after 4 updates. The distribution of newly added collocation points obtained by *SAIS* for the first three iterations

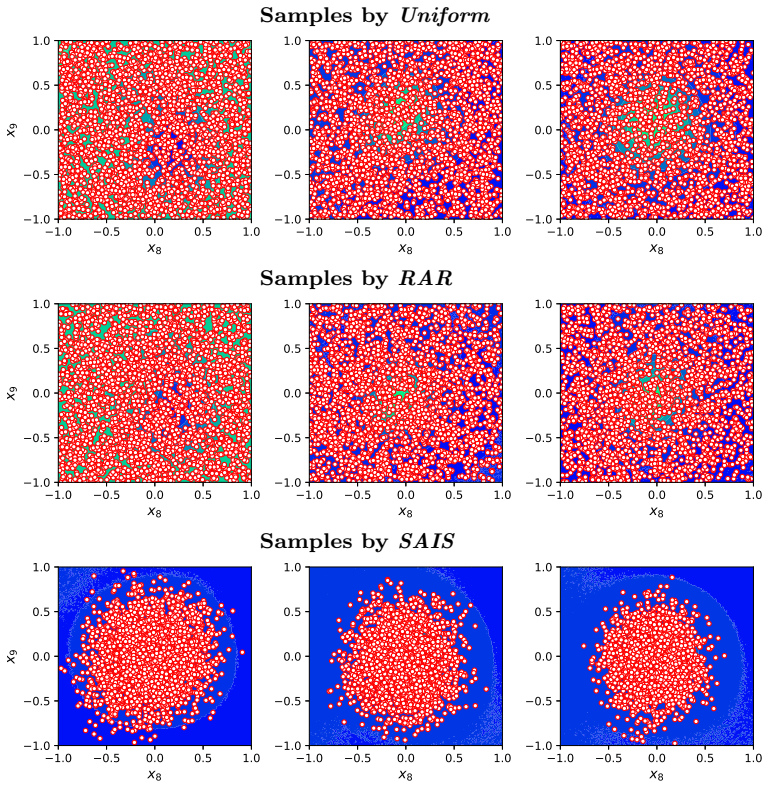


FIGURE 13. The $2nd, 4th, 6th$(from left to right) samples distribution of x_8, x_9 obtained by the three sampling strategies respectively; $d = 9$

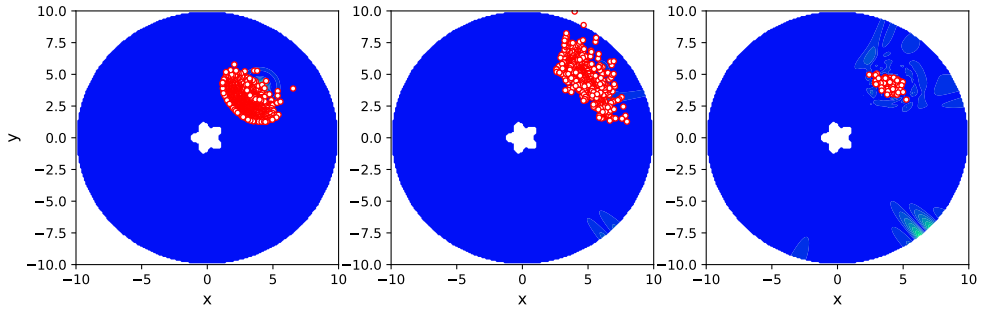


FIGURE 14. The distribution of collocation points obtained by SAIS for the first three updates.

is shown in Fig.14. It is seen that the update points produced by *SAIS* are concentrated near the peak $(4, 4)$.

Fig. 15 shows the predicted solution over a disk with a radius of 10. It is seen that the numerical solution match well with the exact solution. We also provide the L_2 errors in Fig. 16 to demonstrate the efficiency of our adaptive framework. The figure shows that, after four updates, our technique can produce a prediction error of only 2.28×10^{-2}. Additionally, the prediction error and predicted failure probability have a similar pattern, making it useful for creating stop criteria.

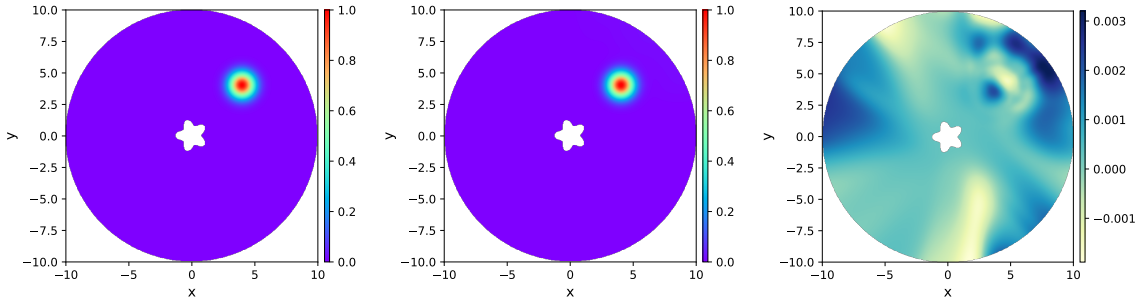


FIGURE 15. The exact solution, numerical solution and absolute error from left to right.

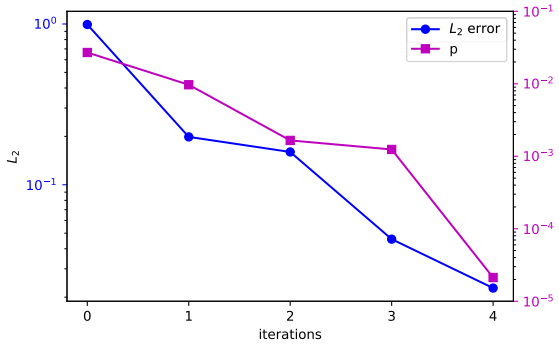


FIGURE 16. The relative L_2 error and the estimated failure probability.

5.6. **Time-dependent problem in an unbounded domain.** We finally consider the following time-dependent equation

$$\begin{aligned} &u_t(x,t) = u_{xx}(x,t) + f(x,t), \quad (x,t) \in \mathbb{R} \times [0,1] \\ &u(x,0) = u_0(x), \quad x \in \mathbb{R}. \end{aligned} \tag{29}$$

We choose the following reference solution

$$u(x,t) = \frac{e^{-\frac{(x-10)^2}{4t+4}}}{\sqrt{t+1}}, \tag{30}$$

In this example, we set the tolerances $\epsilon_r = 0.01$ and $\epsilon_p = 10^{-10}$, respectively. The hyper-parameters used in the *SAIS* algorithm are set to $N_1 = 600, N_2 = 2000, p_0 = 0.05$. The prior distribution of (x,t) is a two dimensional Gaussian distribution with mean vector $\mu_1 = [0,0]$ and covariance matrix $\Sigma_1 = 3I_2$. Moreover, the initial 3000 training points are generated in $[-6,0] \times [0,1]$, which is far away from the peak. The training can be terminated after three updates to the training dataset because the estimated failure probability is smaller than the tolerance (see Fig.18).

The distributions of the collocation points are shown in Fig.17. We can clearly see that the collocation points produced using the *SAIS* algorithm automatically move toward the region where the residual error is the greatest. This phenomenon demonstrates the effectiveness of our FI-PINNs framework in dealing with unbounded time-dependent problems. Moreover, the absolute error showed in Fig.17 gradually decreases during the training process. Finally,

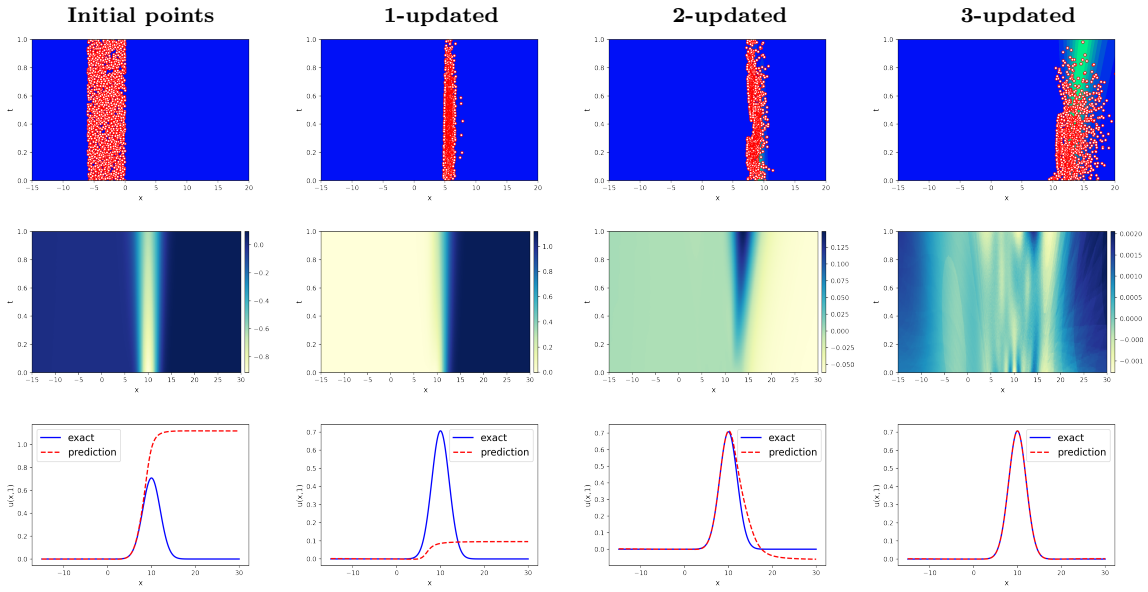


FIGURE 17. From top to bottom: the distribution of (updated) samples, the corresponding absolute error and the predicted values at $t = 1$.

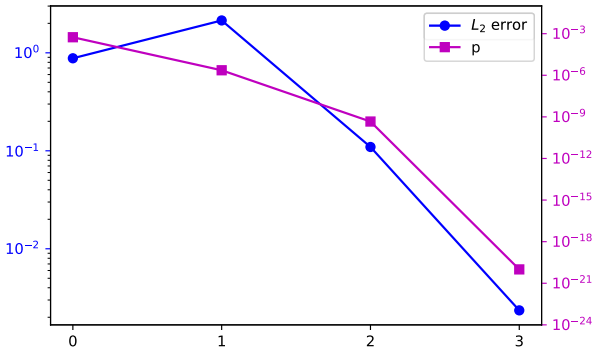


FIGURE 18. The relative L_2 error and the estimated failure probability.

we can obtain an absolute error less than 2×10^{-3} over the whole test domain. To be more clear, we plot the predicted values at $t = 1$. It is obvious that the initial predicted solution differs a lot from the exact solution. While as the training continues, the predicted solution gradually converges to the true solution. After three updates, the relative prediction error shown in Fig.18 is smaller than 3×10^{-3}. The corresponding failure probability shares the same trend. This phenomenon indicates that our FI-PINNs framework and the SAIS sampling strategy are suitable for this kinds of time-dependent problems as well.

6. Concluding remarks

In this work, we present failure-informed PINNs that combine the PINNs with adaptive sampling procedures. The key idea in our FI-PINNs is to define a failure probability as an error indicator, based on the residual. In particular, we propose to use truncated Gaussian

as a simple model to estimate the failure probability and to generate new training points. Rigorous error bound of FI-PINNs is also presented. We illustrate the performance FI-PINNs via several PDE problems that include PDEs with singular solutions, PDEs in unbounded domains, and time-dependent PDEs. It is shown that for all the test problems, FI-PINNs can effectively capture the solution structure. Further studies include applications of FI-PINN to more complex real problems. We remark again here that our truncated Gaussian model can also be changed into more complex models such as Gaussian mixture model. We also mention again that DAS [20] is in fact a more general model for this purpose, for which the main issue is the computational complexity. An optimal way for selecting the density model by balancing the effectiveness and the efficiency will be part of our future studies.

Acknowledgments

LY's work was supported by the NSF of China (No.12171085). TZ's work was supported by the National Key R&D Program of China (No. 2020YFA0712000), the NSF of China (under grant numbers 11822111, 11688101 and 11731006), the Strategic Priority Research Program of Chinese Academy of Sciences (No. XDA25000404), and youth innovation promotion association (CAS).

Appendix A. Further discusses

In this section, we will show two straightforward extensions of the FI-PINNs framework. We shall show in Section A.1 that more general density models such as Gaussian mixture model can be used in our framework. We shall also discuss in Section A.2 how the causality-based weighted residual can be used as a performance function.

A.1. **SAIS using Gaussian mixture model.** The key idea here is to utilize a mixed Gaussian model as the intermediate proposal distribution h_k in our SAIS algorithm. Note that the density function for the Gaussian mixture distribution usually takes the following form:

$$\sum_{m=1}^{M} \pi_m \mathcal{N}(\mu_m, \Sigma_m)$$

where $\mathcal{N}(\mu_m, \Sigma_m)$ is a Gaussian probability density function with mean value μ_m and covariance matrix Σ_m. For every m, $\pi_m \in (0,1)$ satisfy $\sum_{m=1}^{M} \pi_m = 1$. Similar to truncated Gaussian model, we also employ an adaptive method that starts with an initial proposal and incrementally updates the intermediate proposal h_k using samples $\mathcal{D}_k := \{\widetilde{\mathbf{x}}_i^k\}_{i=1}^{N_1}$. How to extract $\mathcal{D}_k$ from the intermediate proposal is completely explained in Section 3.2. Once we have the candidate set $\mathcal{D}_k$, we can estimate the parameters for Gaussian mixture model (π_m, μ_m, Σ_m) using the expectation-maximization (EM) algorithm [1].

In order to demonstrate the effectiveness of the SAIS algorithm with Gaussian mixture model, we consider Example 5.2 with two peaks. We define

$$u(x,y) = e^{-1000[(x-0.5)^2+(y-0.5)^2]} + e^{-1000[(x+0.5)^2+(y+0.5)^2]},$$

as the exact solution, which is shown in Fig.19.

The corresponding numerical results are display in Figs. 20 and 21. We observe very similar behavior for the predicted results as in the earlier experiments: the samples generated by the *SAIS* strategy are concentrated more in the areas where the residual error is high, and the predicted values produced by the *SAIS* strategy closely match the exact solution. This further demonstrates the adaptability of the FI-PINNs framework.

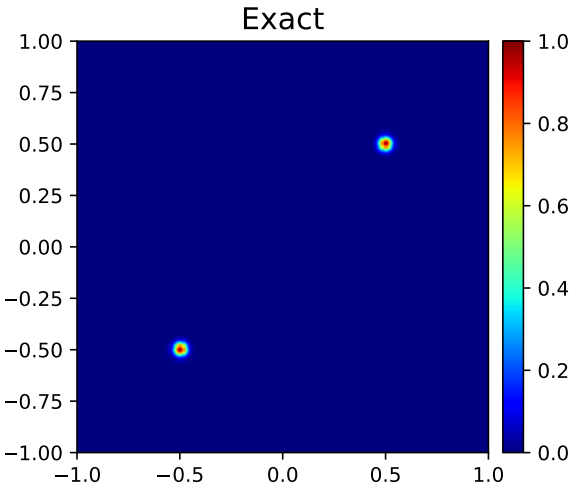


FIGURE 19. Exact solution for the two-dimensional peak test problem.

A.2. **Causal extension of FI-PINNs.** In this section, we present a causal extension of FI-PINNs to deal with time-dependent PDEs. In comparison to FI-PINNs, causal FI-PINNs have two modifications: (1) the *limit-state function* is defined using a causal formulation of the performance function, and (2) the network is trained using a causal weight residual loss. To this end, we divide the whole domain into N_t subdomains in the time direction. Then we can define the weighted residual loss:

$$\mathcal{L}_c(\boldsymbol{\theta}) = \frac{1}{N_t}\sum_{i=1}^{N_t} w_i \mathcal{L}_c\left(t_i, \boldsymbol{\theta}\right), \tag{31}$$

where $\mathcal{L}_c\left(t_i, \boldsymbol{\theta}\right)$ is the residual loss in the ith subdomain and the weights

$$w_i = \exp\left(-\epsilon \sum_{k=1}^{i-1} \mathcal{L}_c\left(t_k, \boldsymbol{\theta}\right)\right), \text{ for } i = 2, 3, \ldots, N_t, \tag{32}$$

where ϵ is a causality parameter. Now we can modify the performance function of FI-PINNs as $\mathcal{Q}(x) = w_i|r(x, t_i)|$, where $r(x, t_i)$ is the residual function in the ith subdomain. Using this performance function, we can define our FI-PINNs framework. We train the network using the weighted residual loss of Eq. (31), just like the causal PINNs[21] do. The proposed method is now refereed to as causal FI-PINNs.

In order to test the effectiveness of the causal FI-PINNs, we consider the following one-dimensional Allen-Cahn equation [21]

$$\begin{aligned} &u_t - 0.0001u_{xx} + 5u^3 - 5u = 0, \quad t \in [0, 1], x \in [-1, 1], \\ &u(0, x) = x^2\cos(\pi x), \\ &u(t, -1) = u(t, 1), \\ &u_x(t, -1) = u_x(t, 1). \end{aligned} \tag{33}$$

We use the same network architectures as in [21] for the NN model, which consists of a fully connected network with 6 hidden layers, each with 128 neurons, and `tanh` as activation function. For ease of use, we also impose periodic boundary conditions as hard

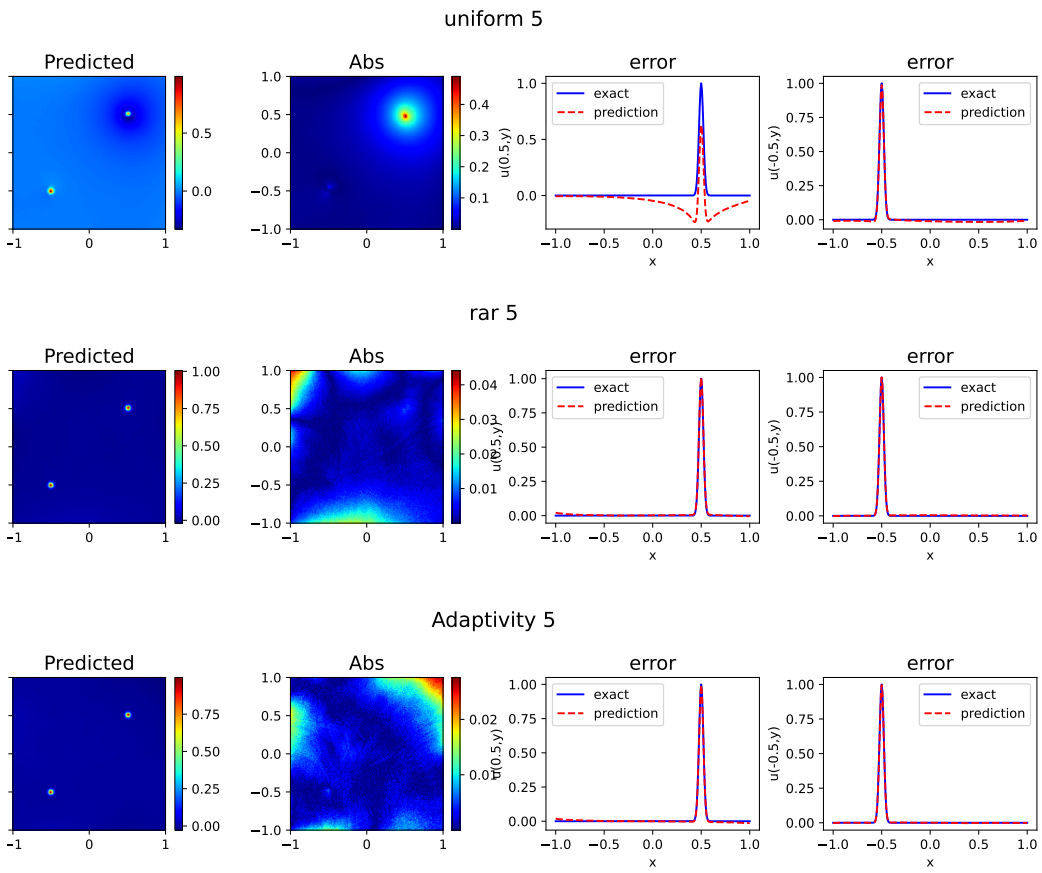


FIGURE 20. The predicted solution, absolute error and the predicted curves at $x = 0.5, -0.5$ obtained by the three different sampling strategies.

constraints. The optimizer is the `Adam` with 20000 iterations. For simplicity, we set the causality parameter $\epsilon = 100$. The initial number of collocation points is 1000. The failure probability tolerance ϵ_p is set to 0.001. In the figures, we will use "*Uniform*" to denote the conventional causal PINNs, "*SAIS*" to denote the causal FI-PINNs algorithm.

The corresponding numerical results are display in Figs. 22- 24. We also compare the predicted error obtained by the conventional FI-PINNs using various sampling techniques, as shown in Table 1. Our causal FI-PINNs strategy, which requires less than 4000 training points, can achieve a prediction error of only 6.5×10^{-3} after 6 updates. The size of training dataset is much smaller than the one used in casual PINNs[21], which achieves the same order of accuracy and save computational cost at the same time. As can be seen, our casual FI-PINNs produce significantly lower predicted error than the conventional casual PINNs when given the same number of training dataset. The relative error was found to be 2.42×10^{-2} for causal PINNs strategy in this case. Uniform training points were used in the original casual PINNs sampling strategy, which resulted in worse predicted error. It should be noted that, in this example, FI-PINNs does not improve numerical results as the *principle of causality* for solving time-dependent PDEs[21].

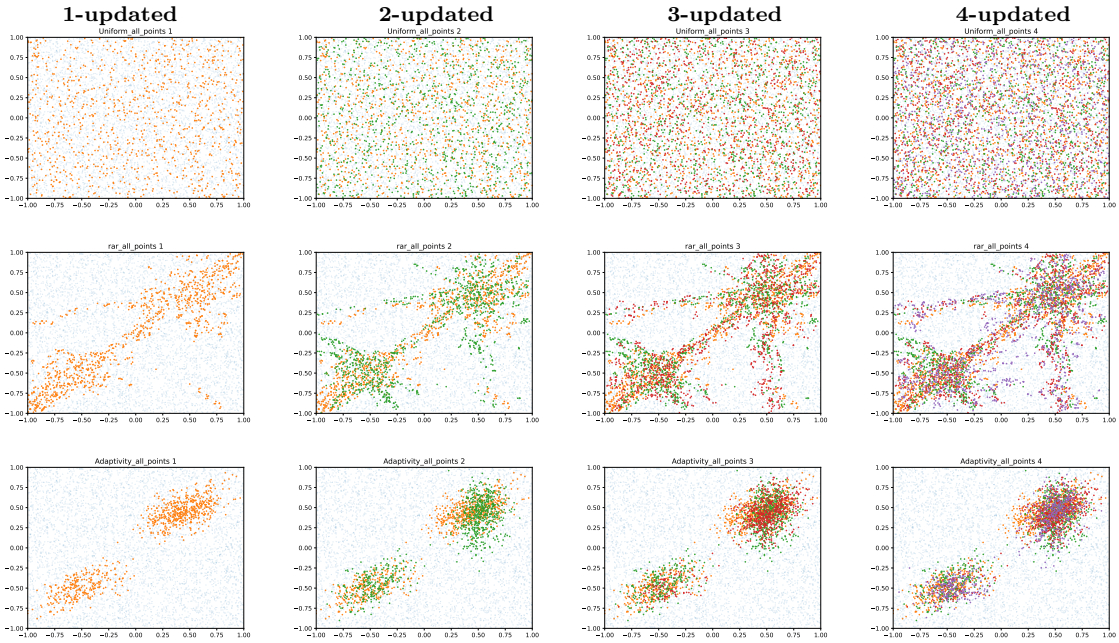


FIGURE 21. The first four updates of the samples distribution obtained using the three sampling strategies: Uniform, RAR and SAIS (from top to bottom).

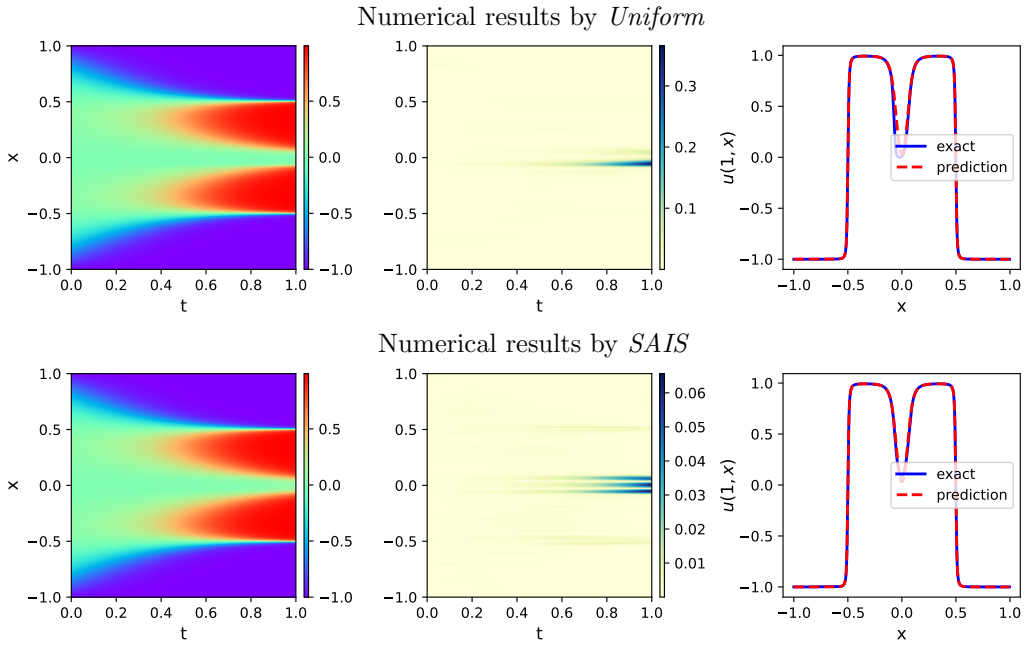


FIGURE 22. Numerical results obtained by different methods.

REFERENCES

[1] CHRISTOPHER M BISHOP AND NASSER M NASRABADI, *Pattern recognition and machine learning*, vol. 4, Springer, 2006.

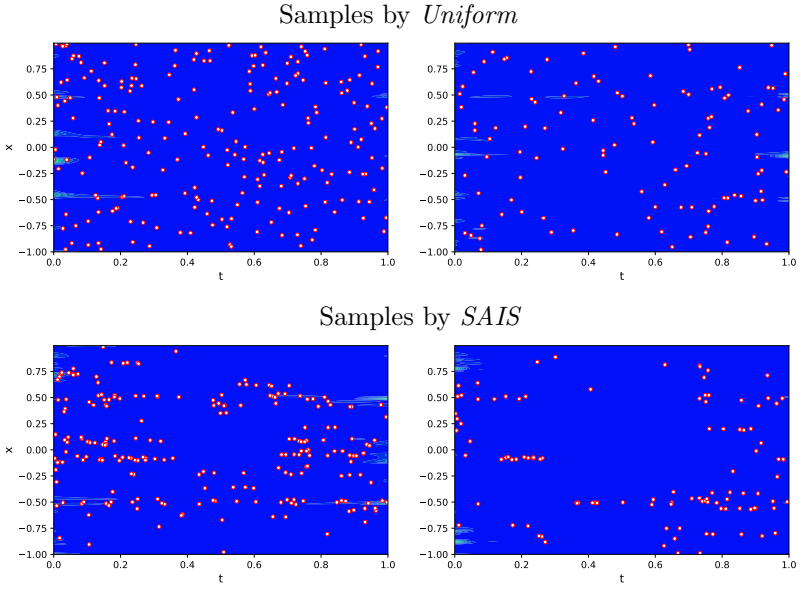


FIGURE 23. The $3th, 5th$ sample distribution (from left to right) obtained by different methods.

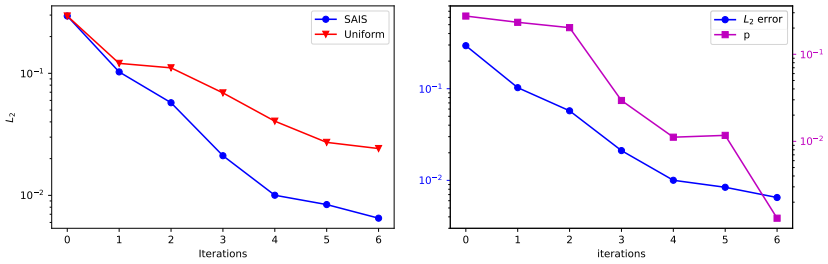


FIGURE 24. Relative L_2 error (left) and the corresponding failure probability (right).

TABLE 1. The final predicted error achieved by different methods.

Method	Relative L_2 error
PINNs	6.79×10^{-1}
FI-PINNs	5.03×10^{-1}
casual PINNs	2.42×10^{-2}
casual FI-PINNs	$\mathbf{6.50 \times 10^{-3}}$

[2] LÉON BOTTOU, *Stochastic gradient descent tricks*, in Neural networks: Tricks of the trade, Springer, 2012, pp. 421–436.
[3] ARKA DAW, JIE BU, SIFAN WANG, PARIS PERDIKARIS, AND ANUJ KARPATNE, *Rethinking the importance of sampling in physics-informed neural networks*, arXiv preprint arXiv:2207.02338, (2022).
[4] WEINAN E, *Machine learning and computational mathematics*, Communications in Computational Physics, 28 (2020), pp. 1639–1670.
[5] WEINAN E AND BING YU, *The deep Ritz method: A deep learning-based numerical algorithm for solving variational problems*, Communications in Mathematics and Statistics, 1 (2018), pp. 1–12.

[6] Xiaodong Feng, Li Zeng, and Tao Zhou, *Solving time dependent fokker-planck equations via temporal normalizing flow*, Communications in Computational Physics, 32 (2022), pp. 401–423.
[7] Wenhan Gao and Chunmei Wang, *Active learning based sampling for high-dimensional nonlinear partial differential equations*, arXiv preprint arXiv:2112.13988, (2021).
[8] Ling Guo, Hao Wu, Xiaochen Yu, and Tao Zhou, *Monte carlo fPINNs: deep learning approach for forward and inverse problems involving high dimensional fractional PDEs*, Comput. Methods Appl. Mech. Engrg., 400 (2022), p. 115523.
[9] Ling Guo, Hao Wu, and Tao Zhou, *Normalizing field flow: solving forward and inverse stochastic differential equations using physics-informed flow model*, J. Comput. Phys., 461 (2022), p. 111202.
[10] Jianguo Huang, Haoqin Wang, and Tao Zhou, *An augmented lagrangian deep learning method for variational problems with essential boundary conditions*, Communications in Computational Physics, 31 (2022), pp. 966–986.
[11] Ameya D Jagtap and George E Karniadakis, *Extended physics-informed neural networks (xpinns): A generalized space-time domain decomposition based deep learning framework for nonlinear partial differential equations.*, in AAAI Spring Symposium: MLPS, 2021.
[12] George Em Karniadakis, Ioannis G Kevrekidis, Lu Lu, Paris Perdikaris, Sifan Wang, and Liu Yang, *Physics-informed machine learning*, Nature Reviews Physics, 3 (2021), pp. 422–440.
[13] Diederik P Kingma and Jimmy Ba, *Adam: A method for stochastic optimization*, arXiv preprint arXiv:1412.6980, (2014).
[14] Aditi Krishnapriyan, Amir Gholami, Shandian Zhe, Robert Kirby, and Michael W Mahoney, *Characterizing possible failure modes in physics-informed neural networks*, Advances in Neural Information Processing Systems, 34 (2021), pp. 26548–26560.
[15] Lu Lu, Xuhui Meng, Zhiping Mao, and George Em Karniadakis, *DeepXDE: A deep learning library for solving differential equations*, SIAM Review, 63 (2021), pp. 208–228.
[16] Levi McClenny and Ulisses Braga-Neto, *Self-adaptive physics-informed neural networks using a soft attention mechanism*, arXiv preprint arXiv:2009.04544, (2020).
[17] Maziar Raissi, Paris Perdikaris, and George E Karniadakis, *Physics-informed neural networks: A deep learning framework for solving forward and inverse problems involving nonlinear partial differential equations*, Journal of Computational physics, 378 (2019), pp. 686–707.
[18] Justin Sirignano and Konstantinos Spiliopoulos, *DGM: A deep learning algorithm for solving partial differential equations*, Journal of computational physics, 375 (2018), pp. 1339–1364.
[19] Shashank Subramanian, Robert M Kirby, Michael W Mahoney, and Amir Gholami, *Adaptive self-supervision algorithms for physics-informed neural networks*, arXiv preprint arXiv:2207.04084, (2022).
[20] Kejun Tang, Xiaoliang Wan, and Chao Yang, *DAS: A deep adaptive sampling method for solving partial differential equations*, arXiv preprint arXiv:2112.14038, (2021).
[21] Sifan Wang, Shyam Sankaran, and Paris Perdikaris, *Respecting causality is all you need for training physics-informed neural networks*, arXiv preprint arXiv:2203.07404, (2022).
[22] Sifan Wang, Yujun Teng, and Paris Perdikaris, *Understanding and mitigating gradient flow pathologies in physics-informed neural networks*, SIAM Journal on Scientific Computing, 43 (2021), pp. A3055–A3081.
[23] Sifan Wang, Xinling Yu, and Paris Perdikaris, *When and why PINNs fail to train: A neural tangent kernel perspective*, Journal of Computational Physics, 449 (2022), p. 110768.
[24] Chenxi Wu, Min Zhu, Qinyang Tan, Yadhu Kartha, and Lu Lu, *A comprehensive study of non-adaptive and residual-based adaptive sampling for physics-informed neural networks*, arXiv preprint arXiv:2207.10289, (2022).
[25] Jeremy Yu, Lu Lu, Xuhui Meng, and George Em Karniadakis, *Gradient-enhanced physics-informed neural networks for forward and inverse pde problems*, Computer Methods in Applied Mechanics and Engineering, 393 (2022), p. 114823.
[26] Yaohua Zang, Gang Bao, Xiaojing Ye, and Haomin Zhou, *Weak adversarial networks for high-dimensional partial differential equations*, Journal of Computational Physics, 411 (2020), p. 109409.